The Cryosphere Discussions

Towards direct coupling of regional climate models and ice sheet models by mass balance gradients: application to the Greenland Ice Sheet

M. M. Helsen, R. S. W. van de Wal, M. R. van den Broeke, W. J. van de Berg, and J. Oerlemans

Institute for Marine and Atmospheric Research Utrecht, P.O. Box 80000, 3508 TA Utrecht, The Netherlands

TCD

5, 2115–2157, 2011

The mass balance gradient method

M. M. Helsen et al.

Title Page

Abstract | Introduction

Conclusions | References

Tables | Figures

◄ | ►

◄ | ►

Back | Close

Full Screen / Esc

Printer-friendly Version

Interactive Discussion

Title Page

Abstract | Introduction

Conclusions | References

Tables | Figures

◄◄ | ►►

◄ | ►

Back | Close

Full Screen / Esc

Printer-friendly Version

Interactive Discussion

Abstract

It is notoriously difficult to couple surface mass balance (SMB) results from climate models to the changing geometry of an ice sheet model. This problem is traditionally avoided by using only accumulation fields from a climate model, and deriving SMB by
5   parameterizing the run-off as a function of temperature, which is often related to surface elevation. In this study, a new parameterization of SMB is presented, designed for use in ice dynamical models to allow a direct adjustment of SMB as a result of a change in elevation (H_s) or a change in climate forcing. This method is based on spatial gradients in the present-day SMB field as computed by a regional climate model. Separate linear
10   relations are derived for ablation and accumulation regimes, using only those pairs of H_s an SMB that are found within a minimum search radius. This approach enables a dynamic SMB forcing of ice sheet models, also for initially non-glaciated areas in the peripheral areas of an ice sheet, and circumvents traditional temperature lapse rate assumptions. The method is applied to the Greenland Ice Sheet (GrIS). Model ex-
15   periments using both steady-state forcing and more realistic glacial-interglacial forcing result in ice sheet reconstructions and behavior that compare favorably with present-day observations of ice thickness.

1   Introduction

Ice dynamical models are a valuable tool to test our understanding of the response
20   of ice sheets to climate changes, and hence in constraining the contribution of large ice sheets to observed fluctuations in sea level changes. In the past decades, various ice sheet model experiments have been carried out for Greenland, to reconstruct ice sheet volume on time scales ranging from centennial to glacial-interglacial scale (e.g. Huybrechts et al., 1991; Letréguilly et al., 1991; Huybrechts, 1994; Van de Wal, 1999b;
25   Marshall and Cuffey, 2000; Lhomme et al., 2005; Otto-Bliesner et al., 2006; Graversen et al., 2010; Robinson et al., 2011). The surface mass balance (SMB) forcing and

Title Page

Abstract | Introduction

Conclusions | References

Tables | Figures

◄ | ►

◄ | ►

Back | Close

Full Screen / Esc

Printer-friendly Version

Interactive Discussion

the coupling to the ice sheet model are of vital importance for the outcome of such experiments (e.g. Letréguilly et al., 1991; Robinson et al., 2011).

However, it is notoriously difficult to constrain the forcing of ice sheet models, due to our limited knowledge of the spatial and temporal character of SMB, which is the complex net result of constantly adjusting fields of accumulation in the interior and melt and subsequent run-off at the margins. Accumulation depends on atmospheric circulation, which changes with climate fluctuations, but also as a consequence of changes in ice sheet elevation and extent. The present-day accumulation pattern is reasonably constrained by both measurements (Bales et al., 2009) and regional climate modelling (Box et al., 2006; Fettweis et al., 2008; Ettema et al., 2009), though uncertainties remain large in areas where measurements are sparse. Melt is a function of the surface energy balance components, which vary widely in space and time over the ice sheet (Van den Broeke et al., 2008b). Part of the melt refreezes in the firn layer as superimposed ice, and thus the amount of run-off depends on the local liquid water balance (Van den Broeke et al., 2008a).

To perform climate experiments with an ice sheet model, assumptions and simplifications are unavoidable for the translation of a time-dependent climate record to spatially and temporally changing forcing fields of surface temperature (T_s) and SMB. With respect to SMB, the classical way to deal with this problem is to separate SMB into accumulation and run-off and estimate both fields separately (e.g. Letréguilly et al., 1991; Huybrechts, 1994; Ritz et al., 1997; Van de Wal, 1999b). The snow accumulation is prescribed by using either a compilation of measurements (e.g. Ohmura and Reeh, 1991; Bales et al., 2009), reanalysis (e.g. Uppala et al., 2005; Robinson et al., 2010), time slice products (e.g. Kiehl and Gent, 2004; Huybrechts et al., 2004; Otto-Bliesner et al., 2006) or scenario runs (e.g. Graversen et al., 2010) from global climate models. To account for climate-related changes in precipitation, a thermodynamic scaling of the accumulation is often applied as a function of a temperature proxy. Run-off is then calculated separately, but highly simplified. The most-often used positive degree-day (PDD) approach relies on a statistical relation between the number of days above

the melting point to the amount of melt (Braithwaite and Olesen, 1989; Reeh, 1991). Combined with assumptions on the amount of superimposed ice formation, run-off is calculated. However, the use of a PDD-model to derive ablation generally leads to overestimation of the climate sensitivity (Van de Wal, 1996), due to non-stationarity of the degree-day factors (Van den Broeke et al., 2010) and not explicitly accounting for changes in e.g. lapse rates and albedo feedbacks in a transient climate (Bougamont et al., 2007). Considering the complexities that determine the spatial and temporal evolution of SMB, the approach to estimate SMB in ice sheet models needs improvement.

Recently the output from climate models is increasingly used as a forcing for numerical ice sheet models. In the process of simulating ice sheet-climate interaction, it would be ideal to have a fully coupled ice sheet-climate model system, but such a coupling set-up is still not feasible due to the large difference in spatial scales and in length of the required model simulations. Ice sheet model experiments describe at least a few millennia of ice sheet evolution, whereas climate models are typically used for a few decades of climate reconstruction. Given these different time scales of the numerical models, asynchronous coupling strategies (e.g. Charbit et al., 2002) are required. Moreover, downscaling techniques (e.g. Robinson et al., 2010; Vizcaíno et al., 2010) are developed to translate climate model fields (often only available on a lower resolution than ice sheet model grids) into useful forcing fields for ice dynamical models. However, SMB is usually not a product of climate models and hence a parameterized calculation of SMB is still required.

Hence, ice sheet-climate interaction simulations will strongly benefit from an unambiguous calculation and use of SMB in a coupled atmosphere-ice sheet model. Here we suggest an alternative approach where SMB fields of a regional climate model are directly coupled, which circumvents assumptions regarding the calculation of run-off. For the present day, mean SMB values are used from the regional climate model RACMO2/GR (Ettema et al., 2009), which can be considered a state-of-the-art SMB field since this product has proved to accurately represent the available measurements. We developed a strategy to account for the height-mass balance feedback as the ice

sheet geometry changes over time, by using spatial SMB gradients as a function of elevation that exist in the present-day distribution over the GrIS.

In Sect. 2 a description is given of the method. Section 3 presents the results obtained for both steady-state experiments and a long climate run for the GrIS over a glacial-interglacial cycle. A discussion follows in Sect. 4 and conclusions are drawn in Sect. 5.

2 Methods

Net SMB would be a very useful forcing field for an ice sheet model. However, the simulated ice sheet will instantly react on its forcings by either advancing or retreating, thereby changing its areal extent and surface elevation (H_s). In turn, this modified ice geometry will have consequences for the SMB pattern via processes such as temperature change, atmospheric circulation, orographic effects, albedo changes, etc. Therefore, using a fixed SMB field as a forcing for an ice sheet model is not realistic for simulations longer than several decades. Similarly as for e.g. the surface temperature (T_s), a lapse rate could be used to make a correction of SMB as a function of H_s.

In the ablation zone we expect the SMB to become less negative with increasing H_s, but the rate of change will vary depending on the partitioning of the surface energy balance during melt, i.e. the sum of net short- and net longwave radiation, and the sensible, latent and subsurface heat fluxes, all evaluated at the surface (Van den Broeke et al., 2008a, 2011). Here we assume that the variability in these terms can be accurately predicted by the local SMB gradient, instead of making it a function of surface temperature as is usually the case in PDD models. In the accumulation zone the behavior of SMB as a function of H_s is even less predictable: SMB can increase due to less ablation, but moving further into the interior SMB will start to decrease with elevation due to decreasing precipitation. To account for these regional differences in SMB patterns, we use surrounding H_s-SMB data for each location over the GrIS to find regional relations that can be applied locally to account for the local height-mass balance feedback. In this way we can account for spatial variability in the relation between H_s

and SMB and it allows us to predict SMB values for locations that can become ice covered, while currently outside the present-day ice mask.

2.1 Spatial mass balance gradients

The climate data we use in this study is the 1958–2007 average SMB from the regional climate model RACMO2/GR (Fig. 1, Ettema et al., 2009). This regional climate model run is forced at its lateral boundaries by 6-hourly data from the global model of ECMWF, using ERA-40 reanalysis (Uppala et al., 2005) up to September 2002 and the operational analysis thereafter. The SMB field is calculated using a physical snow model, allowing an accurate description of refreezing of meltwater and the thermodynamic evolution of the upper snow/firn/ice layers, yielding a realistic reproduction of the present-day SMB distribution with a high horizontal resolution (11×11 km). Note that SMB is only calculated in RACMO2/GR for the area within the ice mask.

For each grid point, pairs of H_s and SMB are determined by selecting the data within a search radius of at least 150 km. A distinction is made between accumulation area and ablation area, and for each regime the search radius is extended in steps of 5 km until a minimum amount of H_s-SMB pairs ($n = 100$) is found. An example of a scatter plot of H_s and SMB data is shown in Fig. 2a, for a location in the ablation zone on the western margin of the GrIS. In this case, a search radius of 150 km is sufficient to find enough grid points in the accumulation area, but for the ablation area the search radius had to be extended to 225 km.

As shown in Fig. 2b, a simple linear regression through all (ablation and accumulation) points does not lead to a useful relation of SMB as a function of H_s. The SMB will then be largely overestimated at high values of H_s, especially for $H_s > 2000$ m. Therefore, we split the accumulation area and the ablation area, and construct separate linear relations for both regimes (Fig. 2c). Furthermore, as one of the boundary conditions of this method we use the constraint that the original SMB value from RACMO2/GR at the specific location should be reproduced given the original elevation, so:

Title Page

Abstract | Introduction

Conclusions | References

Tables | Figures

◄ | ►

◄ | ►

Back | Close

Full Screen / Esc

Printer-friendly Version

Interactive Discussion

$$\text{SMB}(H_{s,ref}) = \text{SMB}_{ref} \tag{1}$$

To this end, the linear regression line is forced through its reference value (green dot in Fig. 2) by adjusting the intercept of the line *after* the regression, without changing its slope. This method ensures a better representation of the SMB gradients then would be obtained with a regression that forces the line through the reference H_s-SMB point, although the linear fits become slightly worse in a statistical sense by this treatment.

Due to the scatter in the H_s-SMB data, an ordinary linear regression does not always result in a good reconstruction of the transition from ablation area to accumulation area, nor does it lead to regression lines that are a good physical representation of the actual H_s-SMB pattern. This is illustrated in Fig. 3, where the dashed lines are the linear regression lines that follow from minimizing the vertical offsets between the data points and the regression line. The reconstructed equilibrium line altitude (ELA) is ∼100 m too high, and the transition height at which the ablation fit crosses the accumulation fit is also much too high. To improve this, instead of minimizing the *vertical* distances, we minimize the *perpendicular* distances between data points and regression line. This method can only be used in scatter plots of data with equal units. To enable this, we first normalize the data on both axes, and then perform a linear regression by minimizing the perpendicular offsets (Fig. 3). Hereafter, regression equations are again rewritten to non-normalized form, such that SMB is predicted by:

$$\text{SMB}(H_s) = \begin{cases} a_{acc} + b_{acc}H_s & \text{if} \quad H_s > H_c \\ a_{abl} + b_{abl}H_s & \text{if} \quad H_s < H_c \end{cases} \tag{2}$$

where H_c is the elevation of intersection between the two lines.

This method works well for a steady-state model run using the present-day climate forcing, when only small SMB adjustments are applied as a function of ice geometry changes. However, when temperature perturbation experiments are performed (see below), SMB patterns in the accumulation area are vulnerable to large changes. This can be due to positive values of b_{acc}, enforcing a positive feedback between H_s and

SMB, that becomes unrealistic with increasing H_s (Figs. 2c and 3a). Negative values of b_{acc} can also lead to problematic SMB values, since these eventually lead to negative SMB values with increasing H_s, which is not likely to occur in Greenland (Fig. 3c). To keep SMB within reasonable boundaries, several minimum and maximum constraints have been tested, and the following were considered most suitable and are introduced for the accumulation regime:

$$SMB_{max} = \max(\overline{SMB_{pos}}, SMB_{ref}) \tag{3}$$

$$SMB_{min} = \begin{cases} 0.25 \times \overline{SMB_{pos}} & \text{if } SMB_{ref} < 0 \\ 0.25 \times SMB_{ref} & \text{if } SMB_{ref} > 0 \end{cases} \tag{4}$$

The black lines in Figs. 2d, 3b and d are examples of the relations that are used to calculate SMB as a function of local H_s. These regressions have been calculated for each grid point within the domain, and results are shown in Fig. 4. The SMB gradients for the accumulation regime (b_{acc} in Eq. 2, Fig. 4b) are generally small ($<0.001\,\text{yr}^{-1}$), and mostly negative over the interior part of the ice sheet, apart from an area in the central north. b_{acc} is positive along the western margin, implying decreasing run-off and/or an increase in accumulation with increasing elevation. The high accumulation in the southeast is reflected by large positive values of the regression constant a_{acc} in this area. Values of b_{abl} show a pattern from high values in the south(-west), to lower values in the north. The gradient of SMB in the western ablation zone is in the order of $\sim 2.5\,\text{m i.e. yr}^{-1}\,\text{km}^{-1}$.

This SBM parameterization allows us to calculate a continuous SMB field over the entire domain, as a function of H_s, also for areas outside the present-day ice mask. This is required to provide the ice sheet model with a continuous SMB forcing, since ice-free areas along the periphery of the ice sheet quickly become ice covered if no negative SMB forcing is applied. Once grid points outside the present-day ice mask becomes ice covered, an SMB value is calculated based on data from currently ice-covered areas in the vicinity of such location. However, while such a location is not (yet)

ice covered, a lower SMB value should be assigned than the value that follows from the parameterization, due to the influence of e.g. a much lower albedo of tundra compared to ice. To account for the influence of the tundra and hence correct for this possible flaw in SMB pattern, we subtract 1 m i.e. yr^{-1} from the calculated SMB when ice thickness is below 1 m. Different values for the treatment of SMB at the ice margin have been tested, and these values prevented an unrealistic expansion of the simulated ice sheet over the entire mainland of Greenland under the present-day SMB forcing.

With this SMB parameterization it is possible to calculate the elevation of intersection (H_c) and the ELA for each individual grid point, assuming a fully ice-covered Greenland mainland for the SMB calculations (Fig. 5). As expected, a north-south gradient is present in both patterns, of decreasing ELA with increasing latitude as this is present in the RACMO2/GR fields. The area with low ELA in the southeast is caused by the high accumulation in this area, prohibiting net ablation on the 11 km ice sheet mask (in reality the ablation zone is 1-several km wide). The east-west gradient over the northern part of the domain is due to the higher accumulation in the northwest compared to the northeast.

2.2 Temperature adjustment by refreezing

Due to the temperature-dependence of the ice viscosity it is of great importance for the ice flow velocity to calculate the ice temperature by solving the thermodynamic equation. The temperature of the ice is determined by the ice advection, diffusion, geothermal heat flux at the bottom, heat production due to ice deformation, friction of the ice at the bottom when its sliding over its bed, and the mean annual temperature at the surface (T_s). Here we use the RACMO2/GR 1958–2007 mean T_s for this latter term, and we correct for elevation changes using the atmospheric lapse rate γ_{atm} (Table 1). Another process that will change the ice temperature is refreezing (R) of percolating meltwater in firn layers. In the more classical treatment of SMB calculation in ice sheet models, R is often calculated on-line as a fraction of the annual ablation by making assumptions about the seasonal cycle of surface temperature and snowpack

characteristics. Hence the heat release that is associated by R can be taken into account in T_s.

In our modelling set up, the effect of R on SMB is already taken into account in the regional climate model, so this effect is included in the net SMB values as we use here. However, we still need to take into account the thermodynamic effect of R for the calculation of ice temperatures. Thus, we can use the refreezing as a separate forcing field (Fig. 6), by applying a relation between R and the associated ice temperature warming as suggested by Reeh (1991):

$$\Delta T_s(R) = 26.6R \tag{5}$$

with R in m w.e. yr^{-1}.

However, using a fixed field of R poses a comparable problem as for SMB, since R will likely change with a changing ice geometry. Hence, we treat this problem in a similar way as we do for SMB, by calculating the gradients of R as a function of H_s, using the same set of data points for each location as were used for the calculation of the SMB(H_s) relations. Figure 7 shows an example of such a relation for a location in the northeast. As constraint for this $R(H_s)$ relation, we demand a positive gradient in the ablation regime, and a negative gradient in the accumulation regime.

2.3 SMB perturbations in climate change experiments

The SMB method as described above is well suited to be used in an asynchronously coupled climate-ice sheet model set-up: the SMB gradients method is used each time step to account for changes in SMB field as a result of ice sheet elevation changes and extent. After a certain integration time of the ice sheet model, the ice sheet surface elevation and extent in the climate model should then be updated by the new H_s field of the ice sheet model, such that the climate model can generate a new climatology over the ice sheet again, which can consequently be used as forcing for the ice sheet model, etc. The method also allows steady-state climate experiments, by modifying the background SMB pattern only for local changes in ΔH_s, which we show below.

However, ice sheet model experiments are often used to simulate the effect of climate perturbations, or reconstruct ice sheet behavior over glacial-interglacial time scale. Therefore, we also intend to test whether the SMB gradients as calculated here can be used to translate a climatic surface temperature perturbation that is applied uniformly over the ice sheet into a spatially differentiated change in SMB. To this end, we extend our method by introducing an extra term in Eq. (2) that accounts for a SMB change as a function of a climate perturbation. Instead of using the actual ice sheet elevation (H_s) in Eq. (2), we use a climatic elevation ($H_{\Delta T}$) that is adjusted as a function of a surface temperature perturbation ($\Delta T_{climate}$):

$$H_{\Delta T} = H_s + \frac{\Delta T_{climate}}{\gamma_{atm}} \tag{6}$$

Hence, for example a climate perturbation of +1 °C and using $\gamma_{atm} = -7.4\,\text{K}\,\text{km}^{-1}$ will lead to a decrease of $H_{\Delta T}$ of 135 m. With a typical SMB gradient of $2\,\text{m i.e. yr}^{-1}\,\text{km}^{-1}$ in the ablation regime this leads to a drop in SMB of $0.27\,\text{m i.e. yr}^{-1}$. Note that since SMB gradients differ spatially, an identical temperature change will lead to regionally different SMB adjustments.

2.4 Ice sheet model

To test this new method of SMB forcing on an ice sheet model for the GrIS, we use the 3-D thermomechanical model ANICE (e.g. Van de Wal, 1999a,b; Bintanja et al., 2005; Bintanja and Van de Wal, 2008; Van den Berg et al., 2008; Graversen et al., 2010) based on the shallow ice approximation (SIA, Hutter, 1983), and including thermodynamics to explicitly account for the temperature-dependent stiffness of the ice. Hence, ice temperature is calculated based on the 3-D advection, diffusion, friction, geothermal heat flux (G) at the bottom and annual surface temperature (T_s) adjusted for the effect of refreezing (Sect. 2.2). The vertical dimension is scaled with the local ice thickness, and consists of 15 layers with increasing resolution near the bed, to accurately account for the large gradient in ice velocity near the bed. For areas where

basal temperatures reach the pressure melting point we allow the ice to slide over its bed, by using a Weertman-type sliding law (Weertman, 1964), corrected for the effect of subglacial water pressure (Bindschadler, 1983). Formation of ice shelves is not allowed; as soon as the ice thickness becomes small enough that it will go afloat and ice
5 is in contact with the ocean, the ice breaks off. As such, calving by means of a flotation criterion is included, but more detailed calving physics are not incorporated explicitly, since model resolution and dynamics are not suited for a more realistic treatment of calving of outlet glaciers. The response of a changing ice load on bedrock elevation is taken into account using an Elastic Litosphere-Relaxing Astenosphere (ELRA) model
10 (Le Meur and Huybrechts, 1996). As such, the ice sheet model is a traditional SIA model including thermodynamics and bedrock adjustment. Table 1 summarizes the values for different parameters used in all components of the ice sheet model.

2.5 Model set up

The different model components (ice flow, thermodynamics, SMB, and bedrock re-
15 sponse) are coupled and applied on a rectangular domain of 141×77 grid points with a grid spacing of 20 km. Bedrock elevation (H_b) and ice thickness (H_i) fields are from Bamber et al. (2001b), and these fields are interpolated to our ice model grid using the mapping package OBLIMAP (Reerink et al., 2010), using an oblique stereographic projection centered at 72° N, 40° W, with projection angle $\alpha = 7.5°$. The same mapping
20 configuration is used to interpolate fields of SMB, T_s and R from the regional climate model RACMO2/GR, and the spatially differentiated functions for $SMB(H_s)$ and $R(H_s)$ are interpolated likewise.

A difference exists between the areal extent of the GrIS ice thickness data as presented in Bamber et al. (2001b) and the arial extent of the ice mask in Bamber et al.
25 (2001a), the latter also containing the spatial distribution of numerous small ice caps and glaciers along the periphery of the GrIS. The differences are especially prominent along the rugged topography along the east coast, e.g. in the area south of Scoresby Sund, where numerous glaciers and ice caps exists, without information on

ice thickness. Since SMB from Ettema et al. (2009) is available for the ice mask from Bamber et al. (2001a), we apply a correction to our initial ice thickness field from Bamber et al. (2001b) by assigning a 10 m thick ice layer to all grid points within the ice mask but where ice thickness data is missing, and let the model freely evolve from there.

Initialization of the 3-D temperature field is done by using the Robin solution based on T_s, G and SMB in the accumulation zone. Ice temperatures in the ablation zone are initialized as a linear profile between T_s and the pressure melting point.

3 Results

3.1 Reference experiment

To test the performance of our parameterizations for SMB and R, we start with a steady-state run of 100 ky using constant present-day forcing, so no additional climate change forcing. Figure 8a shows the evolution of ice volume during this simulation. The ice volume initially quickly increases, from the present-day observed value of 2.90×10^{15} m^3 to 3.20×10^{15} m^3 within 10 ky. After ~30 ky the ice volume has leveled off to its steady-state value of 3.18×10^{15} m^3, 10 % above the observed GrIS volume. It should be noted that only ice on the Greenland mainland has been taken into account; the ice on Ellesmere Island has been removed from this summation.

The dashed black line in Fig. 8a illustrates the results obtained when the effect of refreezing is neglected. This results in a slightly larger ice sheet, due to slightly lower ice temperatures, that influence both deformation rate and the occurrence of sliding. Hence, ice velocity is slightly lower in the non-refreezing experiment, resulting in a slightly higher steady-state ice volume.

Figure 9a shows ice sheet extent and H_s of the steady-state ice sheet after 100 ky, and Fig. 9b illustrates the difference in H_s compared to the present-day state. The ice sheet has advanced along large parts of its margin, especially in the southwest, along its eastern margin and in the north.

The mass balance gradient method

M. M. Helsen et al.

Title Page

Abstract | Introduction

Conclusions | References

Tables | Figures

◄ | ►

◄ | ►

Back | Close

Full Screen / Esc

Printer-friendly Version

Interactive Discussion

The mass balance gradient method

M. M. Helsen et al.

Figure 8b shows the different mass balance terms as a function of time. The term SMB_{pos} and SMB_{neg} contain the integrated values of SMB over the accumulation area and ablation area, respectively. Hence these terms cannot be compared with the ice-sheet integrated accumulation and run-off terms. The steady-state integrated SMB equals $362\,Gt\,yr^{-1}$, and is in balance with the calving flux. This is 23 % lower than the total ice sheet SMB value of $469\,Gt\,yr^{-1}$ from RACMO2/GR (Ettema et al., 2009), and this large difference can be explained by an expansion of the total ablation area, reducing the integrated ice sheet SMB.

The expansion of the ice sheet in the south inevitably occurs due to the high accumulation in combination with the (initial) absence of a significant ablation zone along large stretches of the margin, for example in the southeast (Fig. 1). In reality, most of the ice in this area is lost by calving of fast-flowing outlet glaciers, that export ice to the ocean where it is released by calving. These glaciers flow through deep, narrow fjords that characterize the topography in this area. This process is not well-described in our simulations, due to two reasons: (1) these narrow fjords are not resolved in the 20 km grid, effectively leading to a seaward displacement of the model coastline; and (2) our SIA-type model does neither accurately describe fast flowing glaciers, nor the calving process. This leads to an ice margin advance towards the coast in our simulation, increasing the calving flux, and also allows the formation of an ablation zone in areas that were previously ice-free (Fig. 10). It should be noted here that increasing the resolution to 10 km does not improve the results; outlet glaciers in these fjords have typical widths of less than 5 km.

The pattern of a margin closer to the coast in combination with a slightly thinner interior ice sheet is a typical phenomena that has been found in many ice sheet modelling studies (e.g. Greve, 2005; Graversen et al., 2010; Robinson et al., 2010). The thinner ice sheet interior can be explained by the fact that we have performed a steady-state experiment, whereas the present-day GrIS is not in steady-state with the current climate, and thus consists of colder ice that deforms at a lower rate.

The resulting mass balance pattern (Fig. 10) is in good agreement with the original fields (Fig. 1), which is not surprising as it is based on the RACMO2/GR run for present-day SMB, though elevations are slightly different. Differences occur along the eastern margin where lower SMB values are reconstructed due to higher elevations in combination with negative SMB gradients in the accumulation area. Reconstructed SMB is higher than the original values in the western ablation area, where ice sheet elevations are again higher, but here the SMB gradients are positive.

3.2 Temperature perturbations

As a first indication of the performance of our method, the ice-sheet integrated SMB is assessed as a function of $\Delta T_{climate}$ (Table 2). Obviously, decreasing SMB values are obtained with increasing temperature perturbations. Net SMB becomes negative only at climate perturbations of 4 K and higher, but also for smaller climate perturbations the ice sheet will shrink, as is described below.

A set of temperature-perturbation experiments was carried out, for which the results are shown in Fig. 11. The steady-state ice sheet is perturbed with a certain $\Delta T_{climate}$, for another 100 ky, to reach a new equilibrium state. The perturbation has a direct SMB effect and an indirect (thermo-)dynamic effect on ice volume. The effect of a temperature perturbation on SMB is controlled by Eqs. (2) and (6), and the dominant mechanism is that (obviously) a cooler climate will results in a more extensive accumulation area and smaller ablation rates in the ablation area. However, accumulation areas with negative SMB gradients (b_{acc}) will effectively receive less accumulation, which can regionally result in a net decrease of the integrated SMB.

Both ice sheet extent (Fig. 11a) and ice volume (Fig. 11b) show a clear nonlinear relation with the applied temperature perturbation, with much stronger effects with positive values of $\Delta T_{climate}$. The ice sheet extent hardly increases with lower temperatures, since it almost entirely fills the island of Greenland. Increased ice volume is thus mainly due to thickening of the ice sheet. A slight decrease in ice volume can be identified in the experiments with a temperature perturbations in the range of $\Delta T_{climate} = -5 - 0$ K.

This is due to the decreasing SMB values in the accumulation area, which outweighs the effect of enlargement of the accumulation area.

A huge difference in ice sheet size occurs between the +1 and +2 K experiments. Care must be taken with the quantitative robustness of this result, since it is highly dependent on the the value of γ_{atm} in Eq. (6). However, in a qualitative sense this nonlinear behavior of the GrIS is likely realistic, i.e. that a threshold value exists for the SMB perturbation, above which the GrIS will eventually retreat to only a fraction of its current size. This is in agreement with Van de Wal (e.g. 1999a), who did a set of similar experiments using the same ice dynamical model, but using a different approach to estimate the SMB forcing.

This set of temperature perturbation experiments has also been carried out for a model set-up neglecting the effect of refreezing (not shown). Although the temperature adjustment due to refreezing can be substantial (Fig. 6), the influence of this effect on the final results in terms of ice volume are mostly only minor (see e.g. Fig. 8). However, for certain values of $\Delta T_{climate}$ steady-state ice volume is significantly higher when the effect of refreezing on ice temperature is not taken into account.

3.3 Simulating a full glacial cycle

In analogy with e.g. Letréguilly et al. (1991); Van de Wal (1999a); Greve (2005), we also performed an experiment that aims to describe the GrIS evolution through a full glacial cycle. The climate record used as a proxy for $\Delta T_{climate}$ is based on the GRIP $\delta^{18}O$ record (Johnsen et al., 2001), and converted into a surface temperature deviation following Johnsen et al. (1995). Prior to 105 ky, the GRIP record is not a valid climate proxy due to ice-flow irregularities (North Greenland Ice Core Project members, 2004), so for this period we use the Vostok δD record and blend the two records in a similar may as described in Greve (2005). This temperature forcing is applied uniformly over the domain, and additionally a lapse rate correction on T_s is applied (Table 1). Sea level is prescribed using the reconstructed sea level from Bintanja and Van de Wal (2008). We start our glacial cycle experiment at 128 ky BP, i.e. in the maximum of the Eemian

climate optimum, using the present-day ice thickness as initial conditions, just as in the reference experiment (Sect. 3.1).

Figure 12 shows ice sheet volume as a response on the climate forcing through the glacial cycle. We do not show minimum Eemian ice volume, since no value should be attributed to this value considering the dependence on initial conditions. The simulated increase in ice volume through the glacial culminates in a peak LGM ice volume of $3.56 \times 10^{15}\,\mathrm{m}^3$, which is in the lower range of most earlier reconstructions obtained by ice flow models (e.g. Van de Wal, 1999a; Huybrechts, 2002; Robinson et al., 2010) and paleoclimatic evidence (Fleming and Lambeck, 2004), but slightly higher than the reconstruction by Greve (2005). This low LGM ice volume is a least partly caused by the lack of ice shelf dynamics in our model, prohibiting merging of the GrIS and the Ellesmere Island section of the Laurentide Ice Sheet during the last glacial, which did occur in reality (England, 1999; Alley et al., 2010).

The simulated deglaciation results in a present-day ice sheet volume close to the steady-state volume. Also ice sheet elevation and extent resulting from this climate experiment (Fig. 13) is in reasonable agreement with the observed present-day elevation. Comparison with the steady-state experiment (Fig. 9) shows that a realistic climatic forcing results in an improved ice sheet elevation in the interior. The location of the summit is slightly shifted towards the north, but inland elevations are not underestimated anymore (like in the steady-state experiment, Fig. 9) due to the presence of colder ice and its effect on ice stiffness. Two marginal areas in the southwest and northwest stand out (arrows in Fig. 13) because they are thinner than presently observed, and also contain wide ablation areas with SMB values lower than present (Fig. 14). These areas presently also contain wide ablation areas, which highlights the sensitivity of these areas to surface melting.

4 Discussion

The SMB method as presented here is in principle designed as a tool to improve asynchronous coupling between climate models and ice sheet models, but as shown here it can also be used as a stand-alone SMB forcing module, without multiple couplings to a climate model. To assess the performance of the method, the spatial SMB gradients as used here should ideally be compared with temporal SMB gradients that can be reconstructed from multiple climate model runs using different fields of ice sheet elevation and extent. This is beyond the scope of this study, but will be assessed in future work.

To illustrate the influence of the SMB forcing on the outcome of ice sheet reconstructions, we can however compare this method with the performance of a PDD model. Choices of parameterizations in the PDD model are made such that the resulting ice sheet integrated value of SMB_{PDD} is in good agreement with the present-day observed value reported by Ettema et al. (2009) (Appendix A). The grey lines in Figs. 2d, 3b and 3d show SMB functions resulting from this PDD method. Values of SMB_{PDD} are calculated using different values of mean annual temperature as input for the PDD model, but to facilitate comparison with the SMB gradient method, the results are plotted as a function of elevation, using γ_{atm} to translate ΔT_s to H_s. Generally, the PDD method results in steeper SMB gradients in the ablation regimes, which results in larger ablation rates with decreasing elevation. The example of Fig. 2d also shows that the PDD method does not reproduce the higher positive SMB values as currently found higher up in the accumulation regime, due to a too strong decrease of the accumulation with increasing elevation.

Figure 15 shows a comparison of the SMB pattern calculated by the PDD model (Appendix A) as obtained for the present-day ice sheet with the SMB field from Ettema et al. (2009). The width of the ablation area in the southwestern margin is underestimated by the PDD method, while the melt area as predicted by the PDD method is larger along the northern margin. The spatial pattern in the differences with the

SMB field from Ettema et al. (2009) (Fig. 15b) suggest that the PDD method results in steeper SMB gradients. This has consequences for any applied climate perturbation, as can also be concluded from Table 2, that shows that differences in ice-sheet integrated SMB values increase with increasing magnitude of the climate perturbation.

5 When the steady-state climate perturbation experiments are repeated using the PDD method (crosses in Fig. 11), several differences can be identified. Maximum ice sheet volumes are found for smaller negative values of $\Delta T_{\text{climate}}$, while the SMB gradient method results in a slight decrease of ice volume for these $\Delta T_{\text{climate}}$ experiments due to decreasing SMB in the accumulation area. A decrease of ice volume due to decreasing

10 precipitation also occurs in the PDD method, but only becomes the dominant effect at large negative temperature perturbations. Results for the positive temperature perturbations are particularly different for the +2 K scenario, where the PDD forcing allows for a steady-state GrIS volume of intermediate size ($\sim 1.7 \times 10^{15}\,\text{m}^3$), whereas using the SMB gradient forcing results in a nearly total GrIS retreat. Not surprisingly, applying the

15 PDD forcing for the glacial cycle experiment also results in a different reconstruction (grey line in Fig. 13).

Comparing the results obtained by the different SMB methods cannot distinguish which of the methods gives best results, but it merely illustrates the large importance of the SMB forcing on the outcome of GrIS model simulations. Therefore, the best

20 approach for correct estimation of changes in the SMB as a result of changes in ice sheet elevation and extent is to use frequent coupling between the ice sheet model and a (regional) climate model. The SMB gradient method is designed to be used in between these couplings, with the assumption that regional SMB variability is a better predictor of the adjustment in SMB due to ice sheet geometry changes, rather then a

25 correlation between temperature and SMB (as is done in the PDD approach).

Simulated ice sheet volume and extent resulting from this study are within the range of known reconstructions with similar ice sheet models. A note on the excess of ice along the (predominantly eastern) margin is warranted here. It seems a persisting feature in ice sheet model reconstructions (e.g. Greve, 2005; Graversen et al., 2010;

Robinson et al., 2010), which has become more prominent since improved bedrock topography (Bamber et al., 2001b) and improved climate fields (e.g. Ettema et al., 2009) have become available. The east coast of Greenland consists of rugged terrain, and receives relatively high amounts of precipitation. The narrow ablation area is too small to be properly resolved and to keep the ice margin in place, inducing glacial advance in the model in the direction of the coast. Once glaciated, this area remains covered with ice. Improvements can be expected from model grids that have <1 km resolution, resolving the narrow fjords, in combination with higher order ice sheet models, with better description of fast outlet glacier dynamics, and possibly resolving steeper SMB gradients near the ice margin.

5 Conclusions

We have presented a novel approach to use SMB fields from regional climate models as a forcing for ice sheet models, accounting for the height-mass balance feedback within an ice sheet model simulation. Using the spatial relation between elevation and SMB, a distributed field of SMB gradients is calculated, both for the accumulation regime and the ablation regime, such that SMB values can be retrieved as a function of elevation for each regime, and over the entire domain. It enables a dynamic SMB forcing of ice sheet models, also for initially non-glaciated areas in the peripheral areas of an ice sheet. The method is applied to the Greenland Ice Sheet (GrIS). Model experiments using both steady-state forcing and more realistic glacial-interglacial forcing result in ice sheet reconstructions and behavior that compare favorably with present-day observations.

Appendix A

PDD method

To facilitate comparison of our results obtained with the SMB gradient method with
results from a PDD model, we also performed experiments driven with SMB fields
from a PDD-model, which is briefly described here. This method relies on a statistical
relationship between positive air temperatures and melt rates of snow and ice (e.g.
Braithwaite and Olesen, 1989; Reeh, 1991). When using a PDD model, a suite of
choices exist in parameterizations that can be used to drive the model. Here we made
these choices such that the PDD model produced an ice sheet integrated SMB value
in close agreement with the SMB from RACMO2/GR on the initial ice sheet mask.

We allow the degree-day factors to be different for snow and ice, and also for warm
and cold climate conditions, using the expressions from Tarasov and Peltier (2002).
Following Greve (2005), we assume warm climate conditions south of 72° N. PDDs
are calculated on a monthly basis, based on a sinusoidal temperature cycle over a
year, in combination with a statistical air temperature fluctuation ($\sigma = 5.2$, Tarasov and
Peltier, 2002) to account for random temperature fluctuations and the daily cycle. The
semi-analytical solution by Calov and Greve (2005) is used to calculated the positive
degree-day integral.

To avoid any discrepancy in forcing, we also use RACMO2/GR 1958–2007 mean
T_s to drive the PDD model. Superimposed on this the seasonal temperature cycle is
estimated using the parameterization from Huybrechts and de Wolde (1999). Recently
Fausto et al. (2009) suggested improved parameterizations of surface temperature over
Greenland, but using these resulted in large deviations of the resulting SMB values with
respect to the RACMO2/GR fields.

For accumulation we use 1958–2007 mean precipitation fields (Ettema et al., 2009),
from which we calculate a rain fraction based on the time near-surface temperature is
above +2 °C (Huybrechts and de Wolde, 1999). To account for precipitation changes

Full Screen / Esc

Printer-friendly Version

Interactive Discussion

in different climate settings, the present-day precipitation climatology is adjusted as a function of ΔT_s (Huybrechts and de Wolde, 1999).

The liquid water that is formed (rain and meltwater) is allowed to refreeze, to form superimposed ice, with a maximum based on the cold content of the surface snow layer (Huybrechts and de Wolde, 1999).

References

Alley, R. B., Andrews, J. T., Brigham-Grette, J., Clarke, G. K. C., Cuffey, K. M., Fitzpatrick, J. J., Funder, S., Marshall, S. J., Miller, G. H., Mitrovica, J. X., Muhs, D. R., Otto-Bliesner, B. L., Polyak, L., and White, J. W. C.: History of the Greenland Ice Sheet: Paleoclimatic insights, Quaternary Sci. Rev., 29, 1674–1790, 2010. 2131

Bales, R. C., Guo, Q., Shen, D., McConnell, J. R., Du, G., Burkhart, J. F., Spikes, V. B., Hanna, E., and Cappelen, J.: Annual accumulation for Greenland updated using ice core data developed during 2000–2006 and analysis of daily coastal meteorological data, J. Geophys. Res., 114, D06116, doi:10.1029/2008JD011208, 2009. 2117

Bamber, J. L., Ekholm, S., and Krabill, W.: A new, high-resolution digital elevation model of Greenland fully validated with airborne laser altimeter data, J. Geophys. Res., 106, 6733–6745, 2001a. 2126, 2127

Bamber, J. L., Layberry, R. L., and Gogineni, S. P.: A new ice thickness and bed data set for the Greenland ice sheet 1. Measurement, data reduction, and errors, J. Geophys. Res., 106, 33773–33780, 2001b. 2126, 2127, 2134

Bindschadler, R.: The importance of pressurized subglacial water in separation and sliding and the glacial bed, J. Glaciol., 29, 3–19, 1983. 2126

Bintanja, R. and Van de Wal, R. S. W.: North American ice-sheet dynamics and the onset of 100,000-year glacial cycles, Nature, 454, 869–872, 2008. 2125, 2130

Bintanja, R., Van de Wal, R. S. W., and Oerlemans, J.: Modelled atmospheric temperatures and global sea levels over the past million years, Nature, 437, 125–128, 2005. 2125

Bougamont, M., Bamber, J. L., Ridley, J. K., Gladstone, R. M., Greuell, W., Hanna, E., Payne, A. J., and Rutt, I.: Impact of model physics on estimating the surface mass balance of the Greenland ice sheet, Geophys. Res. Lett., 34, L17501, doi:10.1029/2007GL030700, 2007. 2118

5 Box, J. E., Bromwich, D. H., Veenhuis, B. A., Bai, L.-E., Stroeve, J. C., Rogers, J. C., Steffen, K., Haran, T., and Wang, S.-H.: Greenland Ice Sheet Surface Mass Balance Variability (1988–2004) from Calibrated Polar MM5 Output, J. Climate, 19, 2783–2800, 2006. 2117

Braithwaite, R. J. and Olesen, O. B.: Glacier fluctuations and climatic change, chap. Calculation of glacier ablation from air temperature, West Greenland, Kluwer Academic Publishers,
10 Dordrecht, 219–233, 1989. 2118, 2135

Calov, R. and Greve, R.: A semi-analytical solution for the positive degree-day model with stochastic temperature variations, J. Glaciol., 51, 173–175, 2005. 2135

Charbit, S., Ritz, C., and Ramstein, G.: Simulations of Northern Hemisphere ice-sheet retreat: sensitivity to physical mechanisms involved during the Last Deglaciation, Quaternary Sci.
15 Rev., 21, 243–265, 2002. 2118

England, J.: Coalescent Greenland and Innuitian ice during the Last Glacial Maximum – rivising the Quaternary of the Canadian High Arctic, Quaternary Sci. Rev., 18, 421–456, 1999. 2131

Ettema, J., Van den Broeke, M. R., van Meijgaard, E., van de Berg, W. J., Bamber, J. L., Box, J. E., and Bales, R. C.: Higher surface mass balance of the Greenland ice
20 sheet revealed by high-resolution climate modeling, Geophys. Res. Lett., 36, L12501, doi:10.1029/2009GL038110, 2009. 2117, 2118, 2120, 2127, 2128, 2132, 2133, 2134, 2135, 2143, 2148, 2152, 2156, 2157

Fausto, R., Ahlstrøm, A. P., Van As, D., Bøggild, C. E., and Johnsen, S. J.: A new present-day temperature parameterization for Greenland, J. Glaciol., 55, 95–105, 2009. 2135

25 Fettweis, X., Hanna, E., Gallée, H., Huybrechts, P., and Erpicum, M.: Estimation of the Greenland ice sheet surface mass balance for the 20th and 21st centuries, The Cryosphere, 2, 117–129, doi:10.5194/tc-2-117-2008, 2008. 2117

Fleming, K. and Lambeck, K.: Constraints on the Greenland Ice Sheet since the Last Glacial Maximum from sea-level observations and glacial-rebound models, Quaternary Sci. Rev.,
30 23, 1053–1077, 2004. 2131

Graversen, R. G., Drijfhout, S., Hazeleger, W., Van de Wal, R., Bintanja, R., and Helsen, M.: Greenland's contribution to global sea-level rise by the end of the 21st century, Clim. Dynam., 1–16, 2010. 2116, 2117, 2125, 2128, 2133

The mass balance gradient method

M. M. Helsen et al.

Title Page

Abstract	Introduction
Conclusions	References
Tables	Figures

◄ | ►|

◄ | ►

Back | Close

Full Screen / Esc

Printer-friendly Version

Interactive Discussion

Greve, R.: Relation of measured basal temperatures and the spatial distribution of the geothermal heat flux for the Greenland ice sheet, Ann. Glaciol., 42, 424–432, 2005. 2128, 2130, 2131, 2133, 2135

Hutter, K.: Theoretical glaciology: material science of ice and the mechanics of glaciers and ice sheets, Reidel Publ. Co., Dordrecht, 1983. 2125

Huybrechts, P.: The present evolution of the Greenland ice sheet:an assessment by modelling, Global Planet. Change, 9, 39–51, 1994. 2116, 2117

Huybrechts, P.: Sea-level changes at the LGM from ice-dynamic reconstructions of the Greenland and Antarctic ice sheets during the glacial cycles, Quaternary Sci. Rev., 21, 203–231, 2002. 2131

Huybrechts, P. and de Wolde, J.: The dynamic responce of the Greenland and Antarctic ice sheets to multiple century climate warming, J. Climate, 12, 2169–2188, 1999. 2135, 2136

Huybrechts, P., Letréguilly, A., and Reeh, N.: The Greenland ice sheet and greenhouse warming, Palaeogeogr. Palaeocl., 89, 399–412, 1991. 2116

Huybrechts, P., Gregory, J., Janssens, I., and Wild, M.: Modelling Antarctic and Greenland volume changes during the 20th and 21st centuries forced by GCM time slice integrations, Global Planet. Change, 42, 83–105, 2004. 2117

Johnsen, S. J., Dahl-Jensen, D., Dansgaard, W., and Gundestrup, N.: Greenland palaeotemperatures derived from GRIP bore hole temperature and ice core isotope profiles, Tellus, 47B, 624–629, 1995. 2130

Johnsen, S. J., Dahl-Jensen, D., Gundestrup, N., Steffensen, J. P., Clausen, H. B., Miller, H., Masson-Delmotte, V., Sveinbjörndottir, A. E., and White, J.: Oxygen isotope and palaeotemperature records from six Greenland ice-core stations: Camp Century, Dye-3, GRIP, GISP2, Renland and NorthGRIP, J. Quaternary Sci., 16, 299–307, 2001. 2130

Kiehl, J. T. and Gent, P. R.: The Community Climate System Model, Version 2, J. Climate, 17, 3666–3682, 2004. 2117

Le Meur, E. and Huybrechts, P.: A comparison of different ways of dealing with isostasy: examples from modelling the Antarctic ice sheet during the last glacial cycle, Ann. Glaciol., 23, 309–317, 1996. 2126

Letréguilly, A., Huybrechts, P., and Reeh, N.: Steady-state characteristics of the Greenland ice sheet under different climate states, J. Glaciol., 37, 149–157, 1991. 2116, 2117, 2130

Lhomme, N., Clarke, G. K. C., and Marshall, S. J.: Tracer transport in the Greenland ice sheet: constraints on ice cores and glacial history, Quaternary Sci. Rev., 24, 173–194, 2005. 2116

Marshall, S. J. and Cuffey, K. M.: Peregrinations of the Greenland Ice Sheet divide in the last glacial cycle: implications for central Greenland ice cores, Earth Planet. Sc. Lett., 179, 73–90, 2000. 2116

North Greenland Ice Core Project members: High-resolution record of Northern Hemisphere
5   climate extending into the last interglacial period, Nature, 431, 147–151, 2004. 2130

Ohmura, A. and Reeh, N.: New precipitation and accumulation maps for Greenland, J. Glaciol., 37, 140–148, 1991. 2117

Otto-Bliesner, B., Marshall, S. J., Overpeck, J. T., Miller, G. H., Hu, A., and Members, C. L. I. P.: Simulating Arctic climate warmth and icefield retreat in the last interglaciation, Science, 311,
10   1751–1753, 2006. 2116, 2117

Reeh, N.: Parameterization of melt rate and surface temperature on the Greenland ice sheet, Polarforschung, 59, 113–128, 1991. 2118, 2124, 2135, 2148

Reerink, T. J., Kliphuis, M. A., and van de Wal, R. S. W.: Mapping technique of climate fields between GCM's and ice models, Geosci. Model Dev., 3, 13–41, doi:10.5194/gmd-3-13-2010,
15   2010. 2126

Ritz, C., Fabre, A., and Letréguilly, A.: Sensitivity of a Greenland ice sheet model to ice flow and ablation parameters: consequences for the evolution through the last climatic cycle, Clim. Dynamics, 13, 11–24, 1997. 2117

Robinson, A., Calov, R., and Ganopolski, A.: An efficient regional energy-moisture bal-
20   ance model for simulation of the Greenland Ice Sheet response to climate change, The Cryosphere, 4, 129–144, doi:10.5194/tc-4-129-2010, 2010. 2117, 2118, 2128, 2131, 2134

Robinson, A., Calov, R., and Ganopolski, A.: Greenland ice sheet model parameters constrained using simulations of the Eemian Interglacial, Clim. Past, 7, 381–396, doi:10.5194/cp-7-381-2011, 2011. 2116, 2117

25 Tarasov, L. and Peltier, W. R.: Greenland glacial history and local geodynamic consequences, Geophys. J. Int., 150, 198–229, 2002. 2135

Uppala, S. M., Kållberg, P. W., Simmons, A. J., Andrae, U., Bechtold, V. D. C., Fiorino, M., Gibson, J. K., Haseler, J., Hernandez, A., Kelly, G. A., Li, X., Onogi, K., Saarinen, S., Sokka, N., Allan, R. P., Andersson, E., Arpe, K., Balmaseda, M. A., Beljaars, A. C. M., Berg, L.
30   V. D., Bidlot, J., Bormann, N., Caires, S., Chevallier, F., Dethof, A., Dragosavac, M., Fisher, M., Fuentes, M., Hagemann, S., Hólm, E., Hoskins, B. J., Isaksen, L., Janssen, P. A. E. M., Jenne, R., Mcnally, A. P., Mahfouf, J.-F., Morcrette, J.-J., Rayner, N. A., Saunders, R. W., Simon, P., Sterl, A., Trenberth, K. E., Untch, A., Vasiljevic, D., Viterbo, P., and Woollen, J.:

The mass balance gradient method

M. M. Helsen et al.

The ERA-40 re-analysis, Q. J. Roy. Meteorol. Soc., 131, 2961–3012, doi:10.1256/qj.04.176, 2005. 2117, 2120

Van de Wal, R. S. W.: Mass-balance modelling of the Greenland ice sheet: a comparison of an energy-balance and a degree-day model, Ann. Glaciol., 23, 36–45, 1996. 2118

5 Van de Wal, R. S. W.: The importance of thermodynamics for modeling the volume of the Greenland ice sheet, J. Geophys. Res., 104, 3889–3898, 1999a. 2125, 2130, 2131

Van de Wal, R. S. W.: Processes of buildup and retreat of the Greenland ice sheet, J. Geophys. Res., 104, 3899–3906, 1999b. 2116, 2117, 2125

Van den Berg, J., Van de Wal, R. S. W., Milne, G. A., and Oerlemans, J.: Effect of isostasy on
10 dynamical ice sheet modeling: A case study for Eurasia, J. Geophys. Res., 113, B05412, doi:10.1029/2007JB004994, 2008. 2125

Van den Broeke, M., Smeets, P., Ettema, J., and Kuipers Munneke, P.: Surface radiation balance in the ablation zone of the west Greenland ice sheet, J. Geophys. Res., 113, D13105, doi:10.1029/2007JD009283, 2008a. 2117, 2119

15 Van den Broeke, M., Smeets, P., Ettema, J., van der Veen, C., van de Wal, R., and Oerlemans, J.: Partitioning of melt energy and meltwater fluxes in the ablation zone of the west Greenland ice sheet, The Cryosphere, 2, 179–189, doi:10.5194/tc-2-179-2008, 2008b. 2117

Van den Broeke, M. R., Bus, C., Ettema, J., and Smeets, P.: Temperature thresholds for degree-day modelling of Greenland ice sheet melt rates, Geophys. Res. Lett., 37, L18501,
20 doi:10.1029/2010GL044123, 2010. 2118

Van den Broeke, M. R., Smeets, C. J. P. P., and van de Wal, R. S. W.: The seasonal cycle and interannual variability of surface energy balance and melt in the ablation zone of the west Greenland ice sheet, The Cryosphere, 5, 377–390, doi:10.5194/tc-5-377-2011, 2011. 2119

Vizcaíno, M., Mikolajewicz, U., Jungclaus, J., and Schurgers, G.: Climate modification by future
25 ice sheet changes and consequences for ice sheet mass balance, Clim. Dynam., 34, 301–324, doi:10.1007/s00382-009-0591-y, 2010. 2118

Weertman, J.: The theory of glacial sliding, J. Glaciol., 5, 287–303, 1964. 2126

The mass balance gradient method

M. M. Helsen et al.

Title Page

Abstract	Introduction
Conclusions	References
Tables	Figures

|◄ ►|

◄ ►

Back Close

Full Screen / Esc

Printer-friendly Version
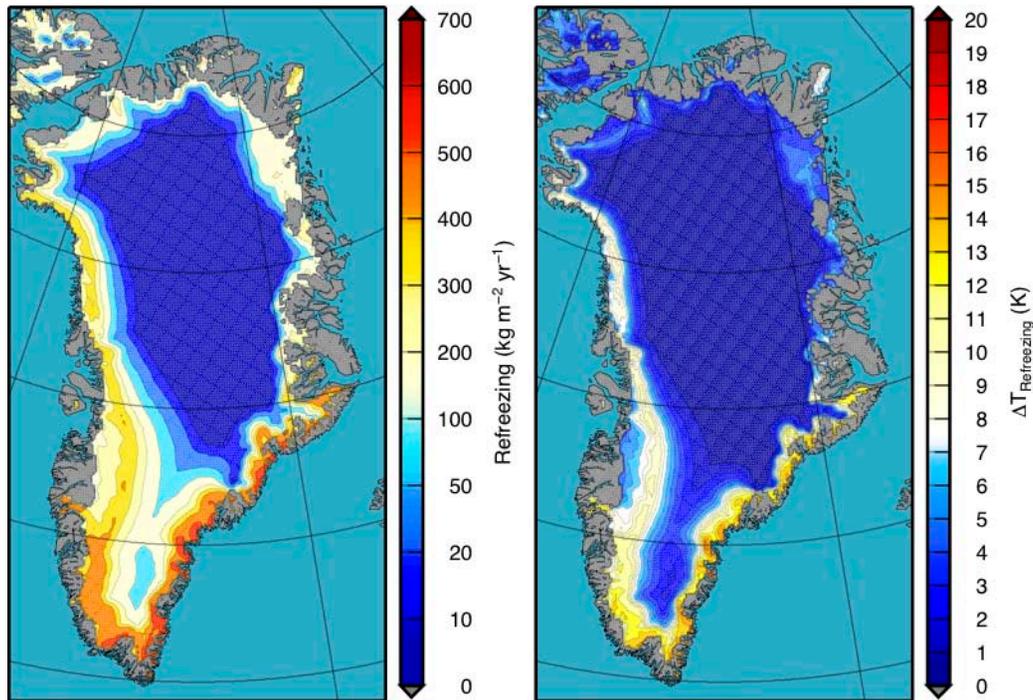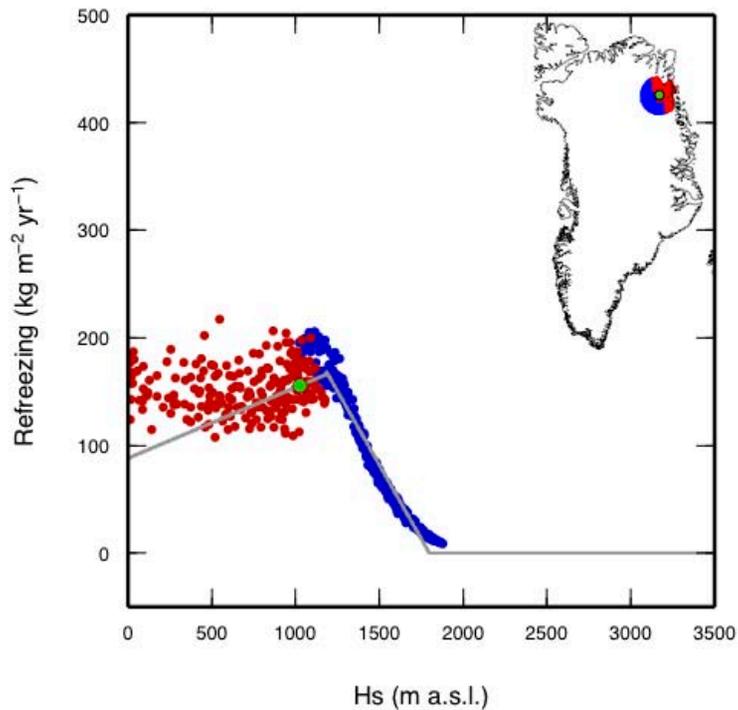
Interactive Discussion

Table 1. Ice sheet model parameter values.

parameter	symbol	value	unit
gravitational acceleration	g	9.81	$\mathrm{m\,s^{-2}}$
ice density	ρ_i	910	$\mathrm{kg\,m^{-3}}$
sea water density	ρ_s	1028	$\mathrm{kg\,m^{-3}}$
Glenn's flow law exponent	n	3	–
flow enhancement	m	3	–
sliding coefficient	A_s	1.8×10^{-10}	$\mathrm{m^8\,N^{-3}\,yr^{-1}}$
geothermal heat flux	G	54.5	$\mathrm{mW\,m^{-2}}$
lithospheric flexural rigidity	D	1×10^{25}	$\mathrm{N\,m}$
astenosphere density	ρ_a	3300	$\mathrm{kg\,m^{-3}}$
bedrock relaxation time	τ	3000	yr
atmospheric lapse rate	γ_{atm}	−7.4	$\mathrm{K\,km^{-1}}$

Table 2. Ice sheet integrated SMB as a function of $\Delta T_{climate}$ using the SMB gradient method and a PDD approach.

$\Delta T_{climate}$ (K)	Ettema09	SMB gradient	PDD
0	469	401	433
+1	–	346	292
+2	–	230	105
+3	–	88	−138
+4	–	−75	−445
+5	–	−262	−834
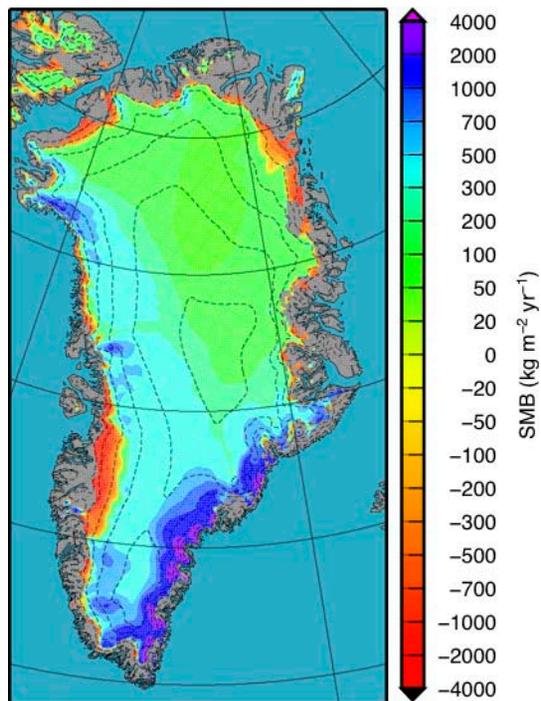
Fig. 1. SMB pattern (1958–2007) over the GrIS (Ettema et al., 2009), dashed contour lines indicate surface elevation in 500 m intervals.
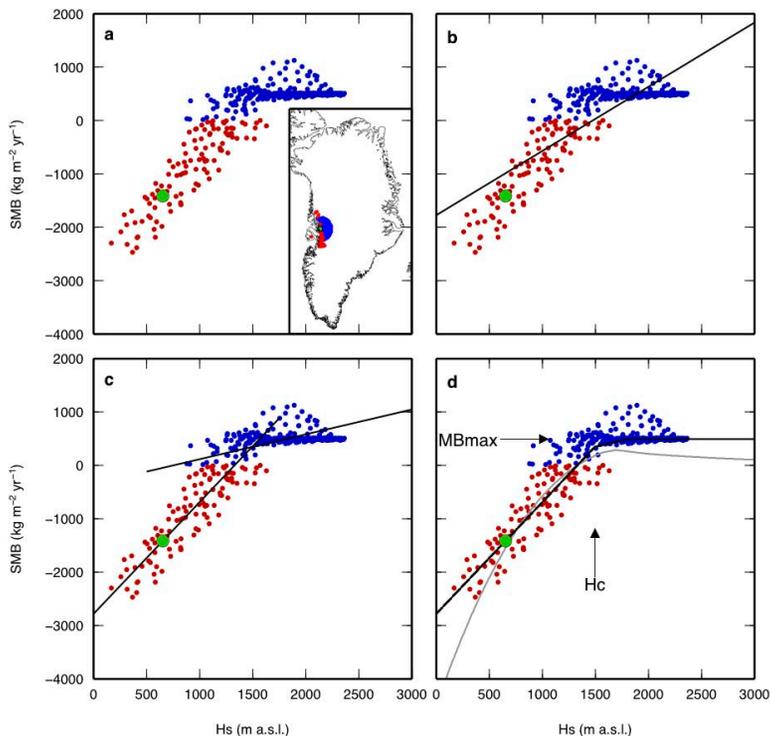
Fig. 2. Example of the construction of the SMB gradient method for a location currently in the ablation area. Blue (red) dots indicate positive (negative) SMB values and locations, green dot indicates reference H_s-SMB value for this grid point and black lines denote relations between SMB and H_s using different methods: **(a)** scatter plot of SMB as a function of H_s; **(b)** simple linear regression; **(c)** using separate regressions for ablation and accumulation regimes; **(d)** final SMB gradient result maximized to a value (MB_{max}) in the accumulation regime. H_c is the elevation of intersection between the accumulation and ablation regime. Grey line represents SMB as calculated by a PDD model.
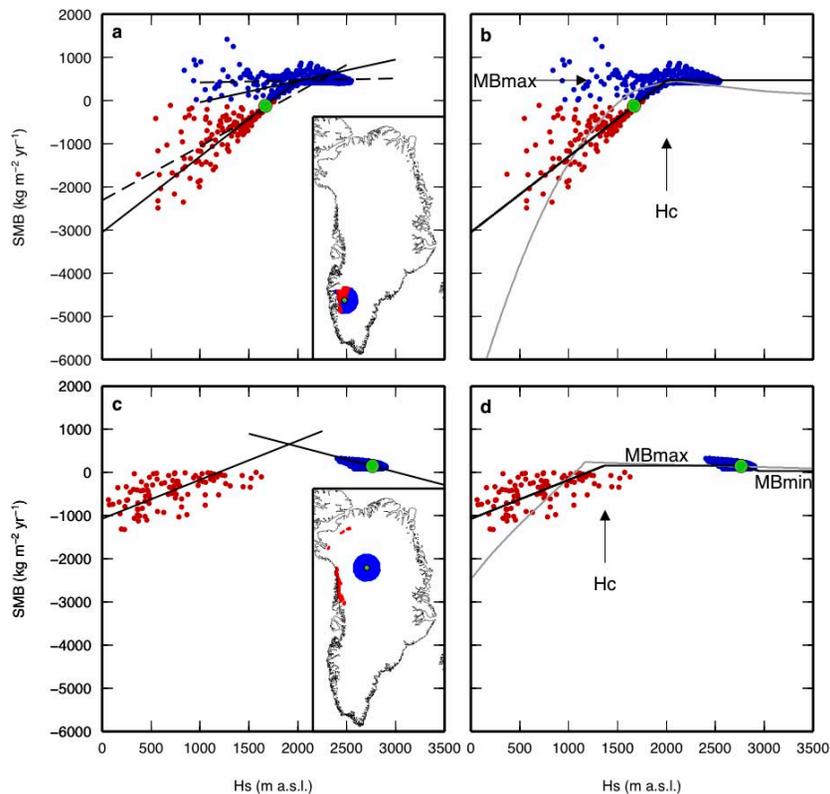
Fig. 3. (a) The effect of the choice between least square linear regression by minimizing vertical offsets (dashed lines) and minimizing perpendicular offsets (solid lines); **(b)** SMB gradients after maximizing the relation for the accumulation regime and forcing the relation for the ablation regime through the reference H_s-SMB values; a negative SMB gradient in the accumulation regime **(c)** illustrates the necessity of introducing a minimum SMB value **(d)** to avoid ablation at high altitudes. Grey line represents SMB as calculated by a PDD model.
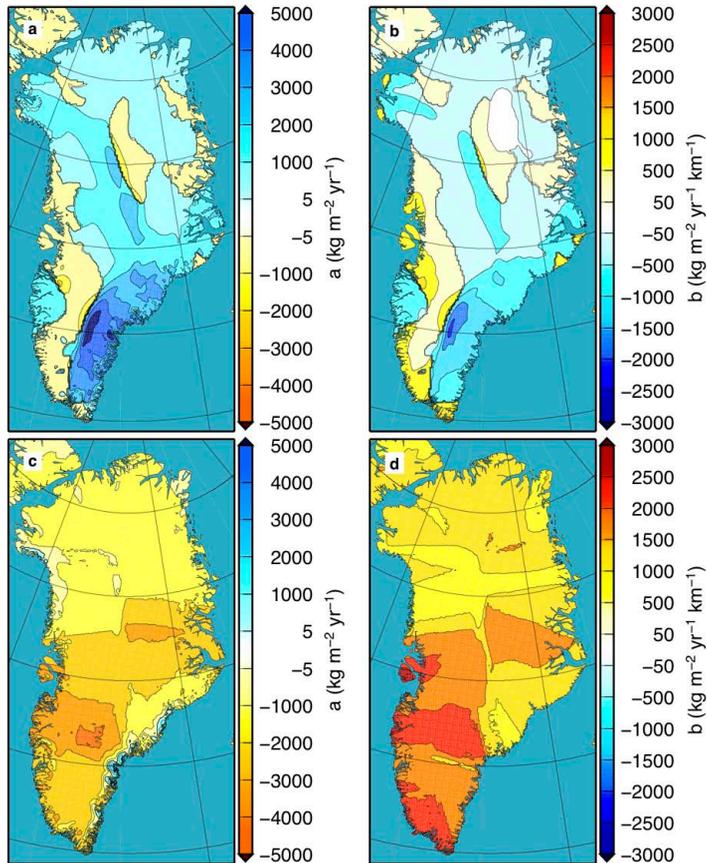
Fig. 4. Fields of coefficients a and b of the spatially varying equation $SMB = a + bH_s$ for the accumulation regime **(a)** and **(b)**, and similarly for the ablation regime **(c)** and **(d)**.
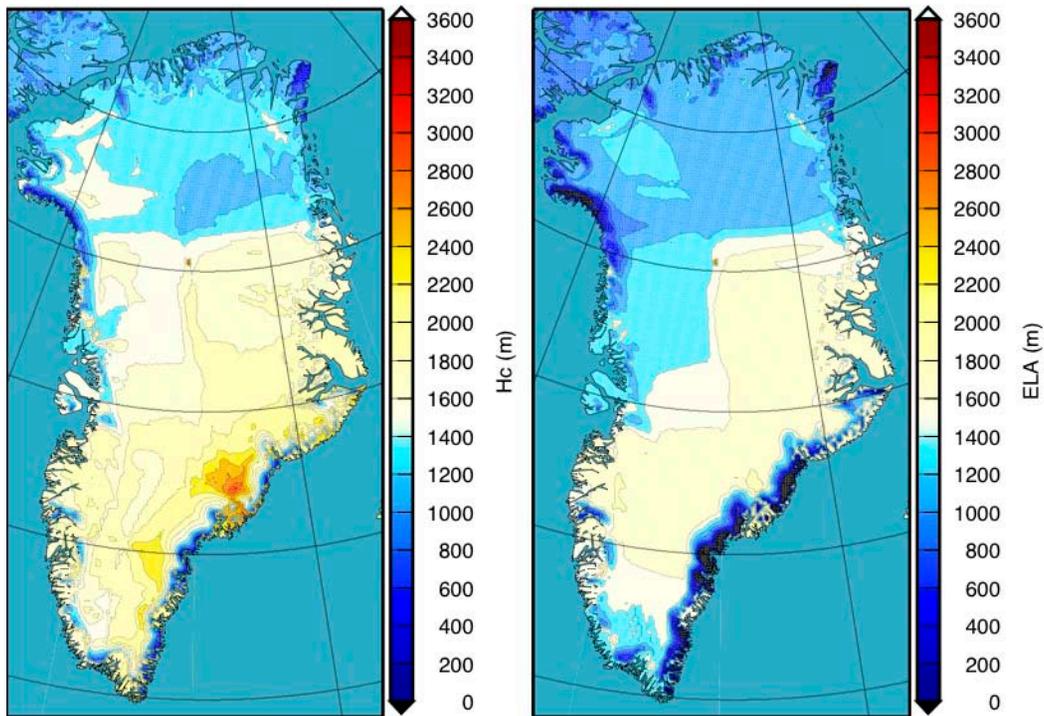
Fig. 5. Elevation of intersection of H_s-SMB relations for ablation and accumulation regimes **(a)** and resulting ELA **(b)** using the H_s-SMB relations.

Title Page

Abstract | Introduction

Conclusions | References

Tables | Figures

|◄ | ►|

◄ | ►

Back | Close

Full Screen / Esc

Printer-friendly Version

Interactive Discussion

Fig. 6. Refreezing from RACMO2/GR (Ettema et al., 2009) **(a)** and the increase in annual mean ice surface temperature **(b)** using the relation by Reeh (1991).

Fig. 7. Parameterization of R as a function of H_s. Location of the data points are shown in the inset.
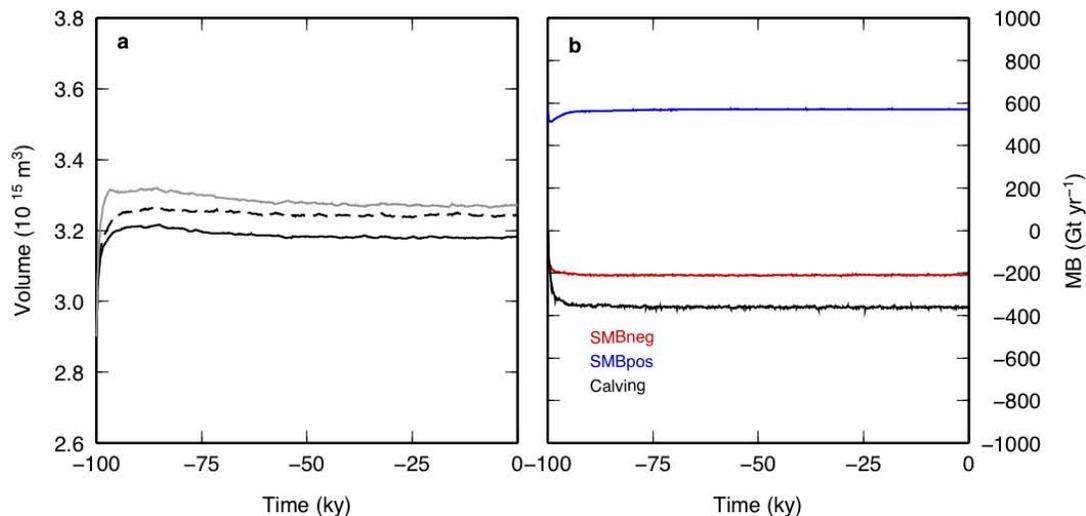
Fig. 8. Time series of **(a)** ice volume for experiments including (black solid line) and excluding (dashed line) refreezing, and using the PDD method (gray line) resulting from a constant climate forcing; **(b)** mass balance (MB) components in the reference experiment (solid black line in panel **a**).
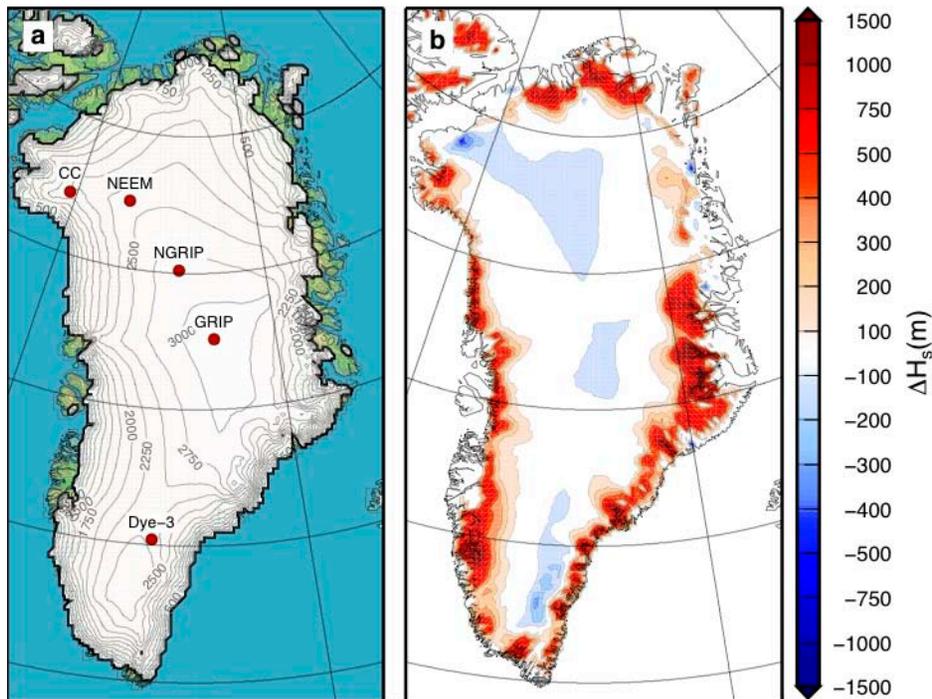
Fig. 9. Steady-state ice sheet elevation **(a)** and difference with present-day observed elevation **(b)** after a 100 ky run using present-day climate forcing and the H_s-SMB gradient method.
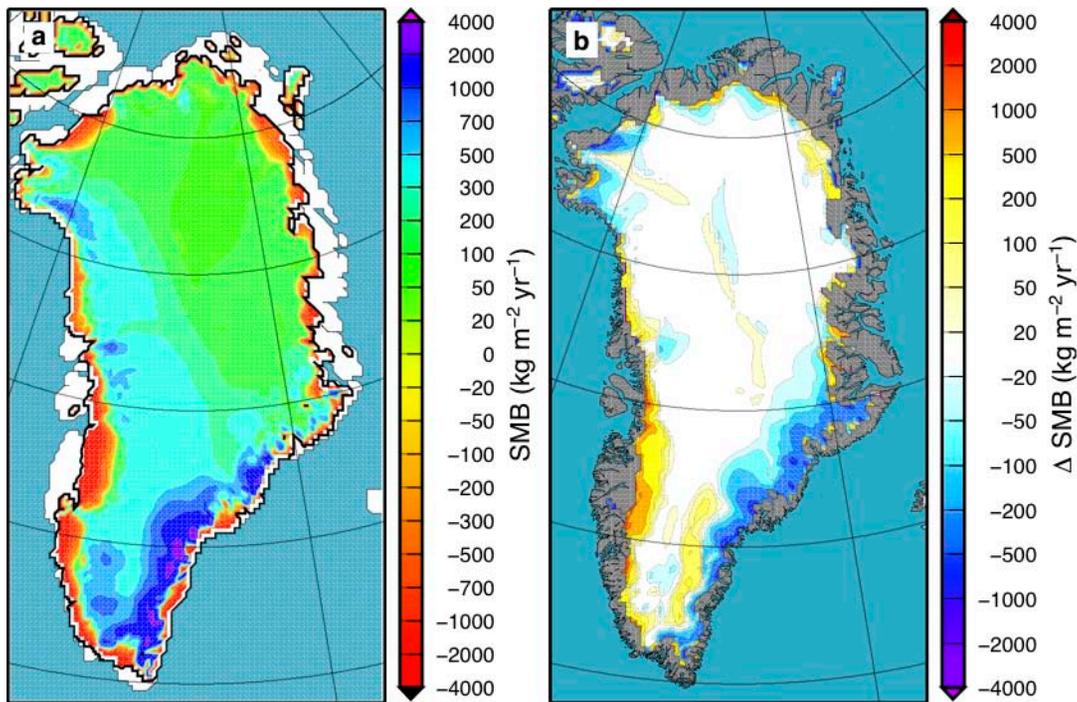
Fig. 10. Steady-state SMB **(a)** and difference with present-day reconstructed SMB from Ettema et al. (2009) **(b)** after a 100 ky experiment using present-day climate forcing and the H_s-SMB gradient method.
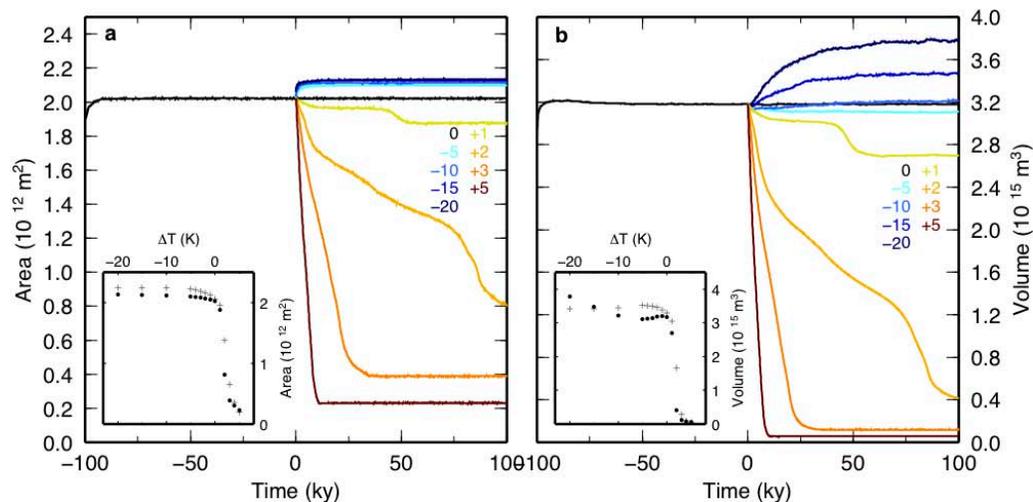
Fig. 11. Time series of ice area **(a)** and volume **(b)** resulting from temperature perturbation experiments using the SMB gradient method. Insets show scatter plots of area and volume as function of applied temperature perturbations using the SMB gradient method (dots) and using the PDD method (crosses).

The mass balance gradient method

M. M. Helsen et al.

Printer-friendly Version

Interactive Discussion
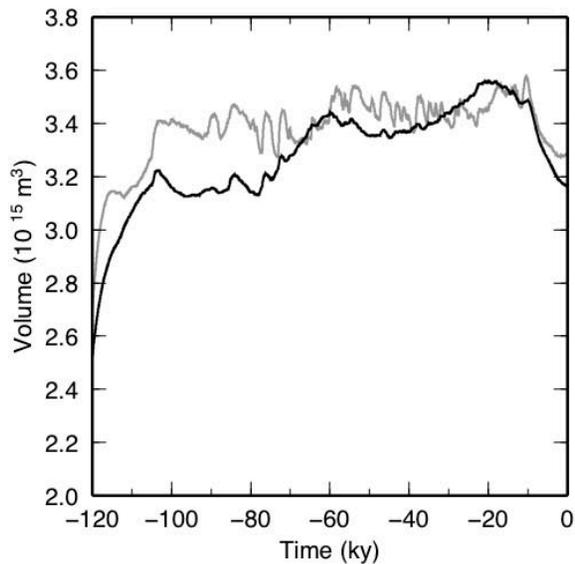
Fig. 12. Ice volume over the last glacial resulting from an experiment using a $\Delta T_{climate}$ forcing from ice core records, using the SMB gradient method (black line) and the PDD method (gray line).
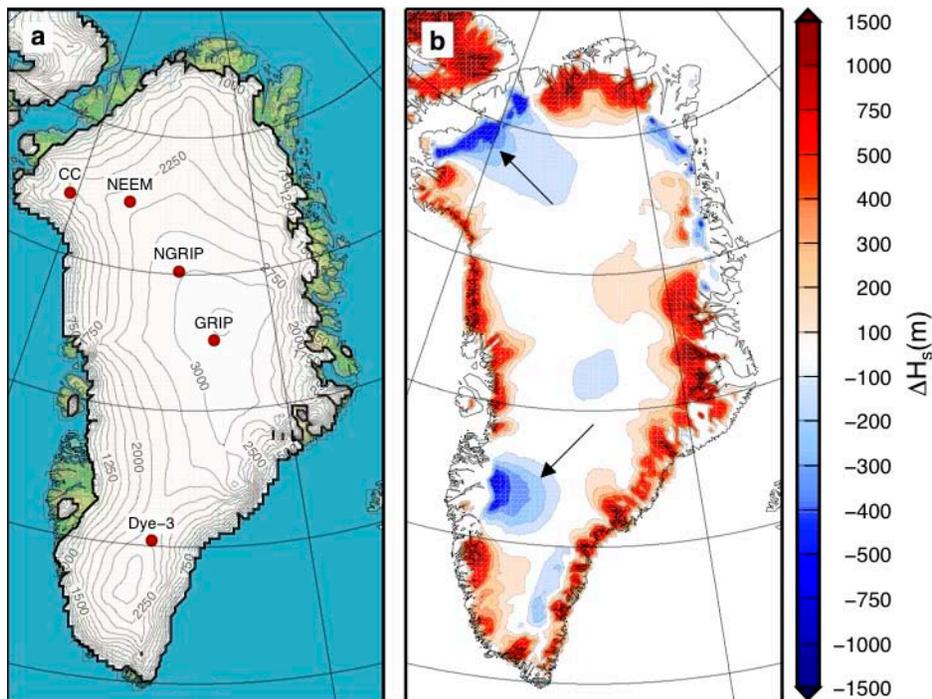
Fig. 13. Ice sheet elevation **(a)** and difference with present-day observed elevation **(b)** after the glacial cycle experiment.
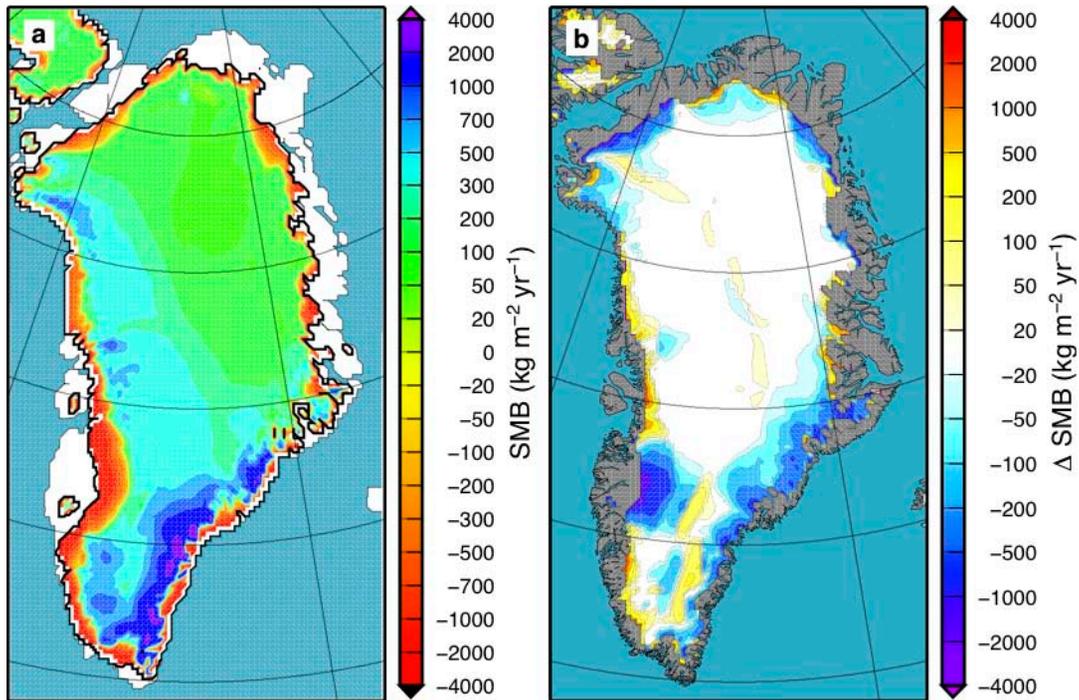
Fig. 14. SMB **(a)** and difference with present-day reconstructed SMB from Ettema et al. (2009) **(b)** after the glacial cycle experiment.
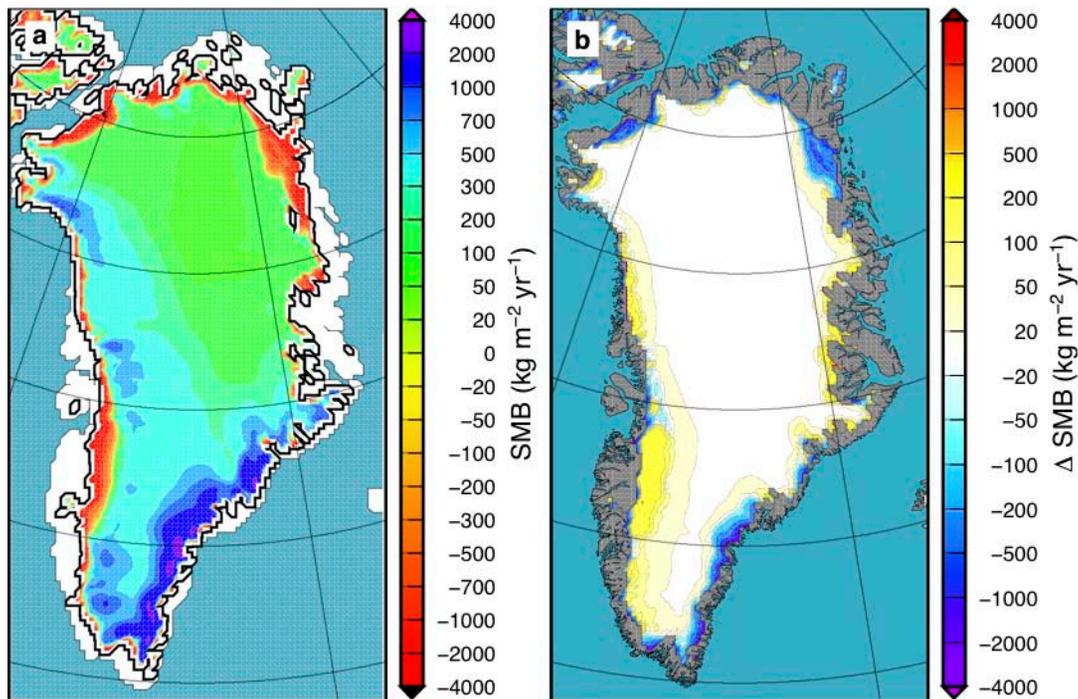
Fig. 15. SMB **(a)** and difference with present-day reconstructed SMB from Ettema et al. (2009) **(b)** resulting from the PDD method, and applied to the present-day observed ice sheet.